

Article

Energy Transfer between Er^{3+} and Pr^{3+} for 2.7 μm Fiber Laser Material

Xiangtan Li ^{1,2}, Binhua Yang ^{1,2,†}, Junjie Zhang ^{3,†}, Lili Hu ^{1,†} and Liyan Zhang ^{1,*}

¹ Key Laboratory of Materials for High Power Laser, Shanghai Institute of Optics and Fine Mechanics, Chinese Academy of Science, Shanghai 201800, China;

E-Mails: lxt_siom2011@foxmail.com (X.L.); yangbinhua07@163.com (B.Y.);

hulili@mail.siom.ac.cn (L.H.)

² Graduate School of Chinese Academy of Science, Beijing 100039, China

³ College of Materials Science and Technology, China Jiliang University, Hangzhou 310018, China;

E-Mail: jjzhang@cjlu.edu.cn

† These authors contributed equally to this work.

* Author to whom correspondence should be addressed; E-Mail: jndxzy@hotmail.com;

Tel.: +86-21-5991-0854; Fax: +86-21-5992-7846.

Received: 1 November 2013; in revised form: 26 December 2013 / Accepted: 30 December 2013 /

Published: 8 January 2014

Abstract: Energy transfer mechanisms between Er^{3+} and Pr^{3+} in $\text{Er}^{3+}/\text{Pr}^{3+}$ codoped germinate glass are investigated in detail. Under 980 nm LD pumping, 2.7 μm fluorescence intensity enhanced greatly. Meanwhile, 1.5 μm lifetime and fluorescence were suppressed deeply due to the efficient energy transfer from $\text{Er}^{3+}:^4\text{I}_{13/2}$ to $\text{Pr}^{3+}:^3\text{F}_{3,4}$, which depopulates the $^4\text{I}_{13/2}$ level and promotes the 2.7 μm transition effectively. The obvious change in J-O parameters indicates that Pr^{3+} influences the local environment of Er^{3+} significantly. The increased spontaneous radiative probability in $\text{Er}^{3+}/\text{Pr}^{3+}$ glass is further evidence for enhanced $^4\text{I}_{11/2} \rightarrow ^4\text{I}_{13/2}$ transition. The $\text{Er}^{3+}:^4\text{I}_{11/2} \rightarrow \text{Pr}^{3+}:^1\text{G}_4$ process is harmful to the population accumulation on $^4\text{I}_{11/2}$ level, which inhibits the 2.7 μm emission. The microscopic energy transfer coefficient of $\text{Er}^{3+}:^4\text{I}_{13/2} \rightarrow \text{Pr}^{3+}:^3\text{F}_{3,4}$ is $42.25 \times 10^{-40} \text{ cm}^6/\text{s}$, which is 11.5 times larger than that of $\text{Er}^{3+}:^4\text{I}_{11/2} \rightarrow \text{Pr}^{3+}:^1\text{G}_4$. Both processes prefer to be non-phonon assisted, which is the main reason why Pr^{3+} is so efficient in $\text{Er}^{3+}:2.7 \mu\text{m}$ emission.

Keywords: 2.7 μm emission; energy transfer micro-parameters; germanate glass

1. Introduction

Mid-infrared laser, especially $\sim 3 \mu\text{m}$ laser, has extensive potential application, such as remote sensing and laser microsurgery. The abundant level systems of Er^{3+} , Dy^{3+} and Ho^{3+} ions make the production of $\sim 3 \mu\text{m}$ laser possible [1–3]. Therefore, a series of methods were used to enhance the intensity of photoluminescence around 2.7 μm , including codoping with other rare-earth ions, such as Tm^{3+} , Nd^{3+} , Yb^{3+} and Pr^{3+} [1,4–8]. Among them, Pr^{3+} is very effective at sensitizing Er^{3+} :2.7 μm emission. Furthermore, $\text{Er}^{3+}/\text{Pr}^{3+}$ codoped tunable CW laser has been obtained in the ZBLAN fiber [9,10]. However, represented by ZBLAN glass, fluoride glass performs with small ΔT ($=T_{x_p} - T_g$, T_{x_p} is the crystallization peak temperature) value, poor chemical and thermal stability, and difficulties in glass preparation and fiber drawing. Researchers have done a lot of work in developing new mid-IR glass to overcome the shortcomings of fluoride glasses. Many results has been reported on chalcogenide, fluorophosphate, tellurite, germanate and $\text{PbO-Bi}_2\text{O}_3\text{-Ga}_2\text{O}_3$ glass [11–15]. Nonetheless, the chalcogenide glass requires a complex fabrication route, especially in refining raw materials and moisture removal process. Besides, the character of bismuth trioxide glass depends on the melting condition. Among the remains of choices, germanate glass does have proper phonon energy and higher glass transition temperature for resisting laser damage. Thus, the $\text{Er}^{3+}/\text{Pr}^{3+}$ codoped germanate glass can have preferable spectroscopic properties as a candidate for 2.7 μm fiber laser material.

Except for Pr^{3+} , no laser output has been reported in other RE^{3+} sensitized Er^{3+} glasses. In order to understand the sensitizing mechanisms of Pr^{3+} to Er^{3+} further, in this work, we studied the energy transfer (ET) dynamics as well as the macroscopic ET parameters in a $\text{Pr}^{3+}/\text{Er}^{3+}$ codoped germanate glass. The energy transfer mechanism in $\text{Er}^{3+}/\text{Pr}^{3+}$ codoped glass is focused to demonstrate the sensitizing effect of Pr^{3+} .

2. Experimental

Glass was prepared following the molar composition $56\text{GeO}_2\text{-}15\text{PbO-}14\text{Na}_2\text{O-}12\text{Ga}_2\text{O}_3\text{-}3\text{PbF}_2\text{-}1\text{Er}_2\text{O}_3\text{-}0.5\text{Pr}_2\text{O}_3$, named GPNG glass. 3 mol% PbF_2 was introduced to reduce the hydroxyl groups. All the high-purity powders were well-mixed and melted at 1150 $^\circ\text{C}$ for 30 min in an electrical furnace. The melting glass was bubbled with high-purity oxygen gas, and then the melts were poured into preheated stainless-steel mold and annealed for 10 h. The homogeneous samples were cut into 20 mm \times 20 mm \times 1 mm and well polished.

Refractive index was measured by a Spectro-Ellipsometer (Woollam W-VASE, error limit $\pm 0.05\%$). With 1 nm steps, the absorption spectra were recorded in the range of 400–1700 nm with a Perkin-Elmer Lambda 900 UV/VIS/NIR spectrophotometer. Under 980 nm, laser diode (LD)'s pumping, fluorescence spectra were tested by a computer-controlled TRIAX 320 type spectrometer and the FLSP920 fluorescence spectrophotometer (Edinburgh Analytical Instruments Ltd., Livingston, UK). The emission spectra ranged in 2550–2800 nm, 1400–1700 nm, 500–700 nm and the lifetime of

$\text{Er}^{3+}:^4\text{I}_{13/2}$ level was also obtained accordingly. The power of 980 nm LD, the width of the slit to collect signals and the position of the samples were fixed to the same condition in the experiment setup in order to accurately compare the intensity of 2.7 μm emission. All the measurements were carried out at room temperature.

3. Results and Discussions

3.1. Absorption Spectra and Infrared Transmittance Spectrum

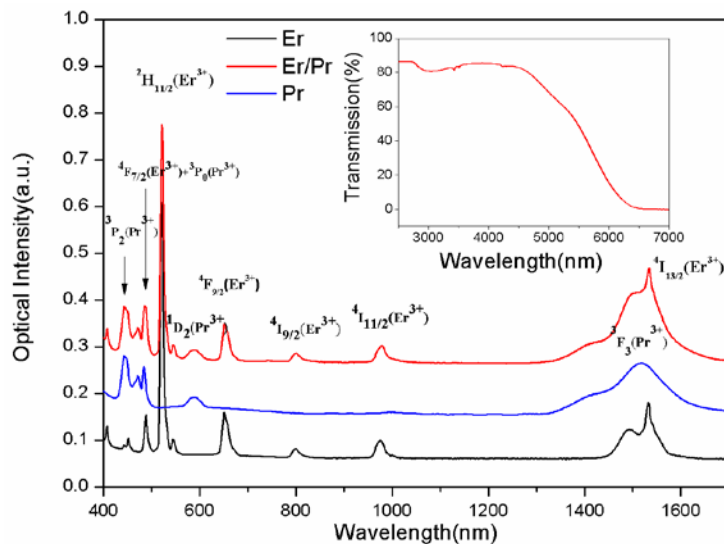
Figure 1 displays the absorption spectra of GPNG glass singly doped with 1 mol% Er_2O_3 , 0.5 mol% Pr^{3+} and coped with both Er_2O_3 and Pr_2O_3 at room temperature. The labeled transitions for both RE^{3+} ions correspond to the ground state to the specific higher levels. The absorption bands at 980 nm illustrate that 980 nm LD can excite this glass.

The mid-infrared transmittance spectrum of $\text{Er}^{3+}/\text{Pr}^{3+}$ codoped sample is shown in the inset of Figure 1. The transmittance reaches 86% and extends to 6.0 μm in the present glass. A typical absorption band of OH^- groups appears at around 3 μm . Due to the overlap with the emission wavelength, the OH^- groups are regarded as a catastrophe in mid-infrared laser materials. The content of OH^- groups can be represented by absorption coefficient, which is defined by:

$$\alpha_{\text{OH}} = -\ln(T_b/T)/l \tag{1}$$

Where l is the sample thickness (cm), T_b and T are the lowest transmittance (%) in OH^- group absorption band and the transmittance of baseline, respectively. The calculated OH^- absorption coefficient is 0.67 cm^{-1} . This peak is small but more work can be done to decrease the OH^- absorption further.

Figure 1. Absorption spectra of Er^{3+} , Pr^{3+} and $\text{Er}^{3+}/\text{Pr}^{3+}$ codoped samples.

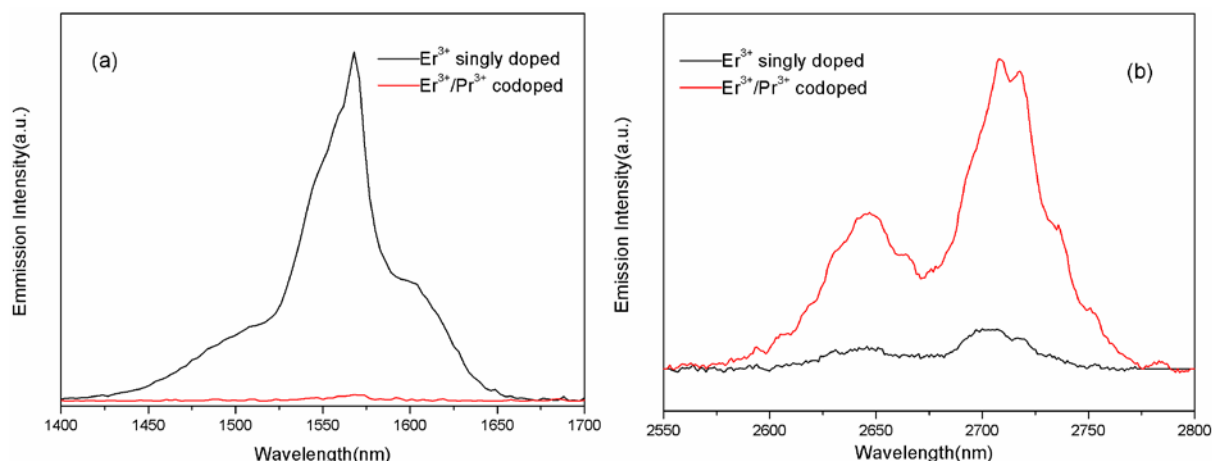


3.2. Fluorescence Spectra and Judd-Ofelt Analysis

Figure 2 shows the measured photoluminescence spectra of Er^{3+} singly doped and $\text{Er}^{3+}/\text{Pr}^{3+}$ codoped GPNG glass that correspond to the $\text{Er}^{3+}:^4\text{I}_{13/2} \rightarrow ^4\text{I}_{15/2}$ and $\text{Er}^{3+}:^4\text{I}_{11/2} \rightarrow ^4\text{I}_{13/2}$ transition,

respectively. It is clearly observed that 2.7 μm emission is significantly enhanced. Meanwhile, the 1.5 μm emission is deeply quenched by Pr³⁺ codoping. In addition, the lifetime of 1.5 μm decrease sharply by Pr³⁺ codoping. The lifetime of Er³⁺:1.5 μm in singly doped sample is 3.23 ms, while that of codoped sample too weak to be detected. According to the previous study [16], this phenomenon suggests that energy transfer occurs between Er³⁺ and Pr³⁺ owing to the equally energetic spacing of multiplet-to-multiplet transitions. Pr³⁺ ions obviously depopulate the Er³⁺:⁴I_{13/2} level in this ET process.

Figure 2. 1.5 μm (a) and 2.7 μm (b) emission in Er³⁺ singly doped and Er³⁺/Pr³⁺ codoped GPNG glasses.



Judd-Ofelt [17] analysis is widely employed to determine the spontaneous emission transition probabilities, radiative lifetime and branching ratios. The Judd-Ofelt intensity parameters of Er³⁺ and Er³⁺/Pr³⁺ glass were calculated in Table 1. Previous studies indicated that Ω₆ is inversely proportional to the covalence of Er-O band. Ω₂ represents symmetry around Er³⁺ ions. In addition, Ω₆ is also related to the optical basic of host materials. Table 1 shows that Ω₂ of GPNG glass is higher than other systems, while Ω₆ is smaller than fluoride and fluorotellurite glass.

Table 1. Judd-Ofelt intensity parameters in various glasses (unit: 10⁻²⁰ cm²).

Parameters	Germanate		Fluorophosphate	Fluoride	Silicate	Fluorotellurite
	Er ³⁺	Er ³⁺ /Pr ³⁺				
Ω ₂	6.60	13.23	5.14 ± 0.10	2.98	4.23	4.38
Ω ₄	1.75	2.81	1.02 ± 0.08	1.40	1.04	3.05
Ω ₆	0.99	2.26	0.91 ± 0.06	1.04	0.61	1.04
Reference	this work		[18]	[19]	[20]	[4]

Theoretically, J-O parameters are influenced by the properties of the host. However, results in this work show that J-O parameters change obviously when Pr³⁺ added in, and this is because the local environment of Er³⁺ has been interfered largely by Pr³⁺, which induces the variations on Ω_{2,4,6}. As a result, the spontaneous radiative probability (A_{rad}) increased from 36.69 s⁻¹ to 60.93 s⁻¹. Moreover, the calculated radiative lifetime of ⁴I_{11/2} level decreased from 4.55 ms to 2.16 ms (Table 2). Obviously, increasing A_{rad} promotes the ⁴I_{11/2}→⁴I_{13/2} transition as well as the 2.7 μm photoluminescence.

Table 2. Calculations of A_{rad} , branching ratio (β) and radiative lifetime in Er^{3+} and Er^{3+}/Pr^{3+} samples.

Initial Level	End Level	Er^{3+}			Er^{3+}/Pr^{3+}		
		A_{rad}	β	τ (ms)	A_{rad}	β	τ (ms)
$^4I_{13/2}$	$^4I_{15/2}$	183.17	100.00%	5.46	334.21	100.00%	2.99
$^4I_{11/2}$	$^4I_{15/2}$	182.92	83.29%	4.55	402.18	86.84%	2.16
	$^4I_{13/2}$	36.69	16.71%		60.93	13.16%	
$^4I_{9/2}$	$^4I_{15/2}$	183.28	77.57%	4.23	297.32	71.91%	2.42
	$^4I_{13/2}$	49.82	21.08%		112.95	27.32%	
	$^4I_{11/2}$	3.19	1.35%		3.19	0.77%	
$^4F_{9/2}$	$^4I_{15/2}$	1882.77	90.80%	0.48	3428.00	90.09%	0.26
	$^4I_{13/2}$	104.40	5.03%		188.15	4.94%	
	$^4I_{11/2}$	80.91	3.90%		178.36	4.69%	
	$^4I_{9/2}$	5.36	0.26%		10.75	0.28%	
$^4S_{3/2}$	$^4I_{15/2}$	1249.87	62.83%	0.50	2853.25	63.07%	0.22
	$^4I_{13/2}$	632.44	31.79%		1443.76	31.91%	
	$^4I_{11/2}$	39.90	2.01%		89.01	1.97%	
	$^4I_{9/2}$	67.14	3.37%		138.05	3.05%	
$^2H_{11/2}$	$^4I_{15/2}$	11581.49			22658.36		
$^4F_{7/2}$	$^4I_{15/2}$	3390.03			7067.49		
$^4F_{5/2}$	$^4I_{15/2}$	779.07			1778.47		
$^2H_{9/2}$	$^4I_{15/2}$	1631.01	33.35%	0.20	3228.73	33.05%	0.10
	$^4I_{13/2}$	2325.23	47.54%		4722.89	48.35%	
	$^4I_{11/2}$	844.79	17.27%		1640.00	16.79%	
	$^4I_{9/2}$	39.18	0.80%		76.81	0.79%	
	$^4F_{9/2}$	50.44	1.03%		99.76	1.02%	

3.3. Energy Transfer Mechanisms between Er^{3+} and Pr^{3+}

Previous study [21] has demonstrated possible mechanisms based on multiplets of Er^{3+} and Pr^{3+} ions in Figure 3. Pumped by 980 nm LD, ground state ions are excited to $^4I_{11/2}$ level (ground state absorption, GSA). The involved energy transfer processes based on the $^4I_{11/2}$ level are as follows: Er^{3+} : $^4I_{11/2} + a \text{ photon} \rightarrow Er^{3+}: ^4F_{7/2}$ (ESA1), $Er^{3+}: ^4I_{11/2} + ^4I_{11/2} \rightarrow Er^{3+}: ^4I_{15/2} + ^4F_{7/2}$ (ETU1), $^4I_{11/2} \rightarrow ^4I_{13/2}$ transition with 2.7 μm emission, and energy transfer from $Er^{3+}: ^4I_{11/2}$ level to $Pr^{3+}: ^1G_4$ level (ET1). After ETU1 and some nonradiative transitions among $^4F_{7/2}$, $^2H_{11/2}$, $^4S_{3/2}$ and $^4F_{9/2}$, the above-mentioned levels are populated. These excited ions contribute to upconversion spectra for green and red emission. Based on lower level $^4I_{13/2}$, $^4I_{13/2} + ^4I_{13/2} \rightarrow ^4I_{15/2} + ^4I_{9/2}$ (ETU2) and nonradiative relaxation from $^4I_{9/2}$ level to $^4I_{11/2}$ level populate the $^4I_{11/2}$. Therefore, the ETU2 process is beneficial to 2.7 μm emission. Moreover, ET2 from $Er^{3+}: ^4I_{13/2}$ to $Pr^{3+}: ^3F_{3,4}$ depletes the $Er^{3+}: ^4I_{13/2}$ level. It is observed that the intensity of red emission is higher than that of green emission in Figure 4. The upper level of red emission ($^4F_{9/2}$) is mainly populated by ESA2: $^4I_{13/2} + a \text{ photon} \rightarrow ^4F_{9/2}$. $^4I_{13/2}$ level is significantly depleted, which is valuable to 2.7 μm emission.

Figure 3. Energy transfer mechanisms of Er³⁺/Pr³⁺ codoped glass.

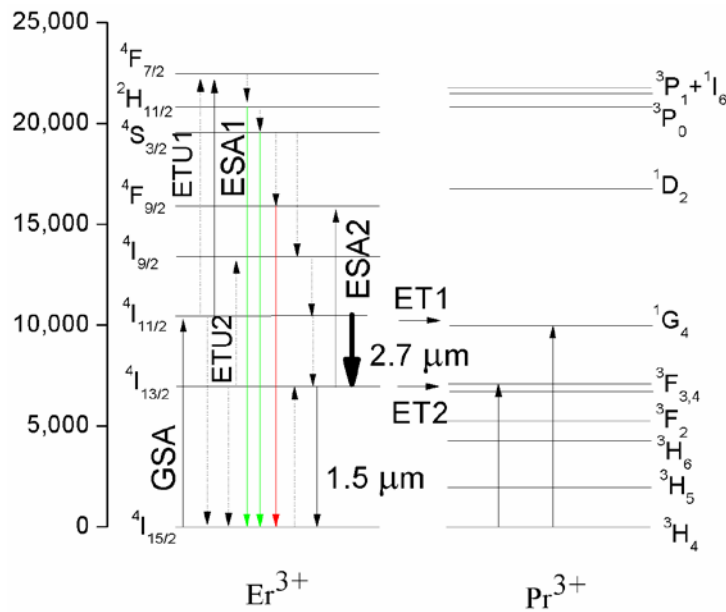
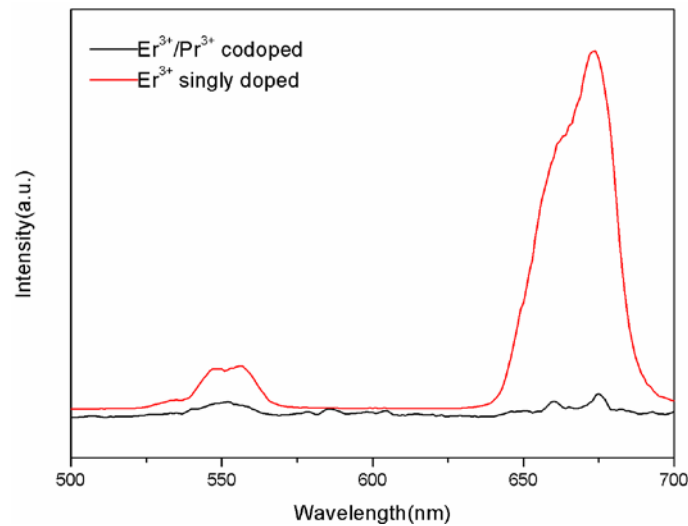


Figure 4. Upconversion spectra of GPNG glasses.



As it mentioned above, codoping with Pr³⁺ can enhance the intensity of 2.7 μm emission through energy transfer processes. To profoundly investigate this system, Forster and Dexter’s [22,23] method is used to quantitatively analyze the energy transfer microscopic parameters between Er³⁺ and Pr³⁺. The energy transfer probability rate between donor (D) Er³⁺ and acceptor (A) Pr³⁺ can be expressed as [24]:

$$W_{D-A} = \left(\frac{2\pi}{\hbar}\right) |H_{DA}|^2 S_{DA}^N \quad (2)$$

Where $|H_{DA}|$ is the Hamiltonian between the donor and acceptor. S_{DA}^N is the integral overlap between m-phonon emission sideband of donor ions and k-phonon absorption line shapes of acceptor ions. N is the total phonons in the transfer process ($m + k = N$). Since m and k have several compound modes, accumulation of different m, k combination is necessary to determinate the integral overlap under N phonon assisted:

$$S_{DA}^N \approx \sum e^{-(S_0^D+S_0^A)} \left[\frac{(S_0^D+S_0^A)^N}{N!} \right] S_{DA}(0,0,E) \delta(N, \frac{\Delta E}{\hbar\omega_0}) \tag{3}$$

$S_{DA}(0,0,E)$ is the overlap between donor emission and acceptor absorption with zero phonon participation. S_0^D and S_0^A are the Huang-Rhys factors in germanate glass. In the resonance and quasi resonance energy transfer process, the overlap S_{DA} is calculated by Miyakawa and Dexter [25]:

$$S_{DA}(m,k,E) \approx \frac{S_0^m S_0^k}{m!k!} e^{-2S_0} S_{DA}(0,0,E) \tag{4}$$

$$S_{DA}(0,0,E) = \int g_{emis}^D(E) g_{abs}^A(E) dE \tag{5}$$

In the case of m-phonon emission by the donor and no phonon absorption by the acceptor, the integral overlap is:

$$\begin{aligned} S_{DA}(m,0,E) &= \int g_{emis(m-phonon)}^D(E) g_{abs}^A(E) dE = \frac{S_0^m}{m!} e^{-S_0} S_{DA}(0,0,E) \\ &= \int \left[\frac{S_0^m}{m!} e^{-S_0} \int g_{emis}^D(E-\Delta E) \right] g_{abs}^A(E) dE \end{aligned} \tag{6}$$

Where $\Delta E = m\hbar\omega_0$, the max phonon energy peak is taken as $\hbar\omega_0$ in glass material. Considering the fact that the measurements are carried out at finite temperature T, the phonon population at T should be counted:

$$\sigma_{emis(m-phonon)}^D = \sigma_{emis}^D(\lambda_m^+) \approx \frac{S_0^m e^{-S_0}}{m!} (\bar{n}+1)^m \sigma_{emis}^D(E-E_1) \tag{7}$$

$$\sigma_{abs(k-phonon)}^A = \sigma_{abs}^A(\lambda_k^-) \approx \frac{S_0^k e^{-S_0}}{k!} (\bar{n})^k \sigma_{abs}^A(E+E_2) \tag{8}$$

Where $E_1 = m\hbar\omega_0$, $E_2 = k\hbar\omega_0$ and $E = E_1 + E_2$. $\lambda_m^+ = 1/(1/\lambda - m\hbar\omega_0)$ and $\lambda_k^- = 1/(1/\lambda + k\hbar\omega_0)$ represent the m-phonon translated wavelength when the donator emits or the acceptor absorbs k-phonon, respectively.

If we just focus on m-phonon creation process, the probability rate of energy transfer can be obtained by:

$$W_{D-A}(R) = \frac{6cg_{low}^D}{(2\pi)^4 n^2 g_{up}^D} \sum_{m=0}^{\infty} e^{-(2\bar{n}+1)} \frac{S_0^m}{m!} (\bar{n}+1)^m \int \sigma_{emis}^D(\lambda_m^+) \sigma_{abs}^A(\lambda_k^-) d\lambda = \frac{C_{D-A}}{R^6} \tag{9}$$

where R is the distance between donor and acceptor. C_{DA} is the energy transfer coefficient, which can represent the efficiency of energy transfer. Thus, C_{DA} can be expressed by:

$$C_{D-A} = \frac{6cg_{low}^D}{(2\pi)^4 n^2 g_{up}^D} \sum_{m=0}^{\infty} e^{-(2\bar{n}+1)} \frac{S_0^m}{m!} (\bar{n}+1)^m \int \sigma_{emis}^D(\lambda_m^+) \sigma_{abs}^A(\lambda_k^-) d\lambda \tag{10}$$

The calculation results by Equations (2)–(10) are listed in Table 3. It also shows the contribution percentage of different phonon numbers to the probability rate involved in the energy transfer. As a result, the transfer coefficient of ET1 $Er^{3+}: {}^4I_{11/2} \rightarrow Pr^{3+}: {}^1G_4$ is 3.67×10^{-40} cm⁶/s while that of ET2:

$\text{Er}^{3+}: {}^4\text{I}_{13/2} \rightarrow \text{Pr}^{3+}: {}^3\text{F}_{3,4}$ is $42.25 \times 10^{-40} \text{ cm}^6/\text{s}$. The coefficient of ET2 is 11.5 times larger than that of ET1; therefore, codoping with Pr^{3+} ions efficiently depletes the lower level of 2.7 μm .

Results also show that non-phonon assisted energy transfer is predominant in the ET process, indicating that energy match is the main reason why Pr^{3+} is very effective in sensitizing $\text{Er}^{3+}: 2.7 \mu\text{m}$ emission.

Table 3. Energy transfer microscopic parameter of Er^{3+} and Pr^{3+} in germanate glass.

Energy Transfer	N (% Phonon Assisted)				Transfer Coefficient ($10^{-40} \text{ cm}^6/\text{s}$)
$\text{Er}^{3+}: {}^4\text{I}_{11/2} \rightarrow \text{Pr}^{3+}: {}^1\text{G}_4$	0	1	2	3	3.67
	55	32	12	1%	
$\text{Er}^{3+}: {}^4\text{I}_{13/2} \rightarrow \text{Pr}^{3+}: {}^3\text{F}_{3,4}$	0	1	2		42.25
	82	15	3%		

4. Conclusions

In summary, $\text{Er}^{3+}/\text{Pr}^{3+}$ codoped GPNG glass has much enhanced 2.7 μm emission and greatly decreased 1.5 μm fluorescence due to the efficient energy transfer from $\text{Er}^{3+}: {}^4\text{I}_{13/2}$ to $\text{Pr}^{3+}: {}^3\text{F}_{3,4}$, which depopulates the ${}^4\text{I}_{13/2}$ level and promotes the ${}^4\text{I}_{11/2} \rightarrow {}^4\text{I}_{13/2}$ transition effectively. Fluorescence lifetime decreases with Pr^{3+} introduction, proving the population evacuation on ${}^4\text{I}_{13/2}$. Interestingly, J-O parameters change obviously, indicating that Pr^{3+} influences the local environment of Er^{3+} significantly. The increased spontaneous radiative probability in $\text{Er}^{3+}/\text{Pr}^{3+}$ glass is further evidence for enhanced ${}^4\text{I}_{11/2} \rightarrow {}^4\text{I}_{13/2}$ transition. Pr^{3+} can also suppress the upconversion luminescence, and this will increase the quantum efficiency of the system. ET process of $\text{Er}^{3+}: {}^4\text{I}_{11/2} \rightarrow \text{Pr}^{3+}: {}^1\text{G}_4$ is harmful to the population accumulation on ${}^4\text{I}_{11/2}$ level, which inhibits the 2.7 μm emission. The calculation of energy transfer microscopic indicates that the transfer coefficient of $\text{Er}^{3+}: {}^4\text{I}_{13/2}$ to $\text{Pr}^{3+}: {}^3\text{F}_{3,4}$ is $42.25 \times 10^{-40} \text{ cm}^6/\text{s}$, which is 11.5 times larger than that of $\text{Er}^{3+}: {}^4\text{I}_{11/2} \rightarrow \text{Pr}^{3+}: {}^1\text{G}_4$, and both processes are preferred to be non-phonon assisted, which is the main reason why Pr^{3+} is so efficient in $\text{Er}^{3+}: 2.7 \mu\text{m}$ emission. This result provides another proof to illustrate the energy transfer mechanisms between Pr^{3+} and Er^{3+} .

Acknowledgments

This research was supported by the Chinese National Natural Science Foundation (No. 51172252, 61177083 and 51372235).

Conflicts of Interest

The authors declare no conflict of interest.

References

1. Chai, G.; Dong, G.; Qiu, J.; Zhang, Q.; Yang, Z. 2.7 μm emission from transparent $\text{Er}^{3+}, \text{Tm}^{3+}$ codoped yttrium aluminum Garnet ($\text{Y}_3\text{Al}_5\text{O}_{12}$) nanocrystals–tellurate glass composites by novel comelting technology. *J. Phys. Chem. C* **2012**, *116*, 19941–19950.

2. Tsang, Y.H.; El-Taher, A.E.; King, T.A.; Jackson, S.D. Efficient 2.96 μm dysprosium-doped fluoride fibre laser pumped with a Nd:YAG laser operating at 1.3 μm . *Opt. Express* **2006**, *14*, 678–685.
3. Jackson, S.D. Single-transverse-mode 2.5-W holmium-doped fluoride fiber laser operating at 2.86 μm . *Opt. Lett.* **2004**, *29*, 334–336.
4. Guo, Y.; Li, M.; Hu, L.; Zhang, J. Effect of fluorine ions on 2.7 μm emission in Er³⁺/Nd³⁺-codoped fluorotellurite glass. *J. Phys. Chem. A* **2012**, *116*, 5571–5576.
5. Wen, L.; Wang, J.; Hu, L.; Zhang, L. Sensitizing effect of Nd³⁺ on the Er³⁺:2.7 μm emission in fluorophosphate glass. *Chin. Opt. Lett.* **2011**, *9*, doi:10.3788/col201109.121601.
6. Sousa, D.F.d.; Sampaio, J.A.; Nunes, L.A.; Baesso, M.L.; Bento, A.C.; Miranda, L.C. Energy transfer and the 2.8- μm emission of Er³⁺ and Yb³⁺ doped low silica content calcium aluminate glasses. *Phys. Rev. B* **2000**, *62*, 3176–3180.
7. Bai, G.; Ding, J.; Tao, L.; Li, K.; Hu, L.; Tsang, Y.H. Efficient 2.7 μm emission from Er³⁺/Pr³⁺ codoped oxyfluorotellurite glass. *J. Non-Cryst. Solids* **2012**, *358*, 3403–3406.
8. Bai, G.; Tao, L.; Li, K.; Hu, L.; Tsang, Y.H. Enhanced light emission near 2.7 μm from Er–Nd co-doped germanate glass. *Opt. Mater.* **2013**, *35*, 1247–1250.
9. Schneider, J.; Hauschild, D.; Frerichs, C.; Wetenkamp, L. Highly efficient Er³⁺: Pr³⁺ codoped CW fluorozirconate fiber laser operating at 2.7 μm . *Int. J. Infrared Millim. Waves* **1994**, *15*, 1907–1922.
10. Coleman, D.J.; King, T.A.; Ko, D.-K.; Lee, J. Q-switched operation of a 2.7 μm cladding-pumped Er³⁺/Pr³⁺ codoped ZBLAN fibre laser. *Opt. Commun.* **2004**, *236*, 379–385.
11. Zhang, L.; Yang, Z.; Tian, Y.; Zhang, J.; Hu, L. Comparative investigation on the 2.7 μm emission in Er³⁺/Ho³⁺ codoped fluorophosphate glass. *J. Appl. Phys.* **2011**, *110*, 093106.
12. Guo, Y.; Li, M.; Tian, Y.; Xu, R.; Hu, L.; Zhang, J. Enhanced 2.7 μm emission and energy transfer mechanism of Nd³⁺/Er³⁺ co-doped sodium tellurite glasses. *J. Appl. Phys.* **2011**, *110*, 013512:1–013512:5.
13. Lin, H.; Chen, D.; Yu, Y.; Yang, A.; Wang, Y. Enhanced mid-infrared emissions of Er³⁺ at 2.7 μm via Nd³⁺ sensitization in chalcogenide glass. *Opt. Lett.* **2011**, *36*, 1815–1817.
14. Song, J.H.; Heo, J.; Park, S.H. Emission properties of PbO–Bi₂O₃–Ga₂O₃–GeO₂ glasses doped with Tm³⁺ and Ho³⁺. *J. Appl. Phys.* **2003**, *93*, 9441–9445.
15. Richards, B.D.O.; Teddy-Fernandez, T.; Jose, G.; Binks, D.; Jha, A. Mid-IR (3–4 μm) fluorescence and ASE studies in Dy³⁺ doped tellurite and germanate glasses and a fs laser inscribed waveguide. *Laser Phys. Lett.* **2013**, *10*, doi:10.1088/1612-2011/10/8/085802.
16. Golding, P.S.; Jackson, S.D.; King, T.A.; Pollnau, M. Energy transfer processes in Er³⁺-doped and Er³⁺,Pr³⁺-codoped ZBLAN glasses. *Phys. Rev. B* **2000**, *62*, 856–864.
17. Feng, X.; Tanabe, S.; Hanada, T. Spectroscopic properties and thermal stability of Er³⁺-doped germanotellurite glasses for broadband fiber amplifiers. *J. Am. Ceram. Soc.* **2001**, *84*, 165–171.
18. Tian, Y.; Xu, R.; Zhang, L.; Hu, L.; Zhang, J. Observation of 2.7 μm emission from diode-pumped Er³⁺/Pr³⁺-codoped fluorophosphate glass. *Opt. Lett.* **2011**, *36*, 109–111.
19. Ivanova, S.; Pellé, F. Strong 1.53 μm to NIR-VIS-UV upconversion in Er-doped fluoride glass for high-efficiency solar cells. *J. Opt. Soc. Am. B* **2009**, *26*, 1930–1938.

20. Zou, X.; Izumitani, T. Spectroscopic properties and mechanisms of excited state absorption and energy transfer upconversion for Er³⁺-doped glasses. *J. Non-Cryst. Solids* **1993**, *162*, 68–80.
21. Coleman, D.J.; Jackson, S.D.; Golding, P.; King, T.A. Measurements of the spectroscopic and energy transfer parameters for Er³⁺-doped and Er³⁺, Pr³⁺-codoped PbO-Bi₂O₃-Ga₂O₃ glasses. *J. Opt. Soc. Am. B* **2002**, *19*, 2927–2937.
22. Dexter, D.L. A theory of sensitized luminescence in solids. *J. Chem. Phys.* **1953**, *21*, 836–850.
23. Förster, T. Intermolecular energy migration and fluorescence (Ger). *Ann. Phys.(Leipzig)* **1948**, *2*, 55–75.
24. Tian, Y.; Xu, R.; Hu, L.; Zhang, J. 2.7 μm fluorescence radiative dynamics and energy transfer between Er³⁺ and Tm³⁺ ions in fluoride glass under 800 nm and 980 nm excitation. *J. Quant. Spectrosc. Radiat. Transf.* **2012**, *113*, 87–95.
25. Miyakawa, T.; Dexter, D.L. Phonon sidebands, multiphonon relaxation of excited states, and phonon-assisted energy transfer between ions in solids. *Phys. Rev. B* **1970**, *1*, 2961–2969.

© 2014 by the authors; licensee MDPI, Basel, Switzerland. This article is an open access article distributed under the terms and conditions of the Creative Commons Attribution license (<http://creativecommons.org/licenses/by/3.0/>).